Nanoscale

ROYAL SOCIETY OF CHEMISTRY

COMMUNICATION

View Article Online
View Journal | View Issue

Cite this: *Nanoscale*, 2023, **15**, 101

Received 5th October 2022,
Accepted 24th November 2022

DOI: 10.1039/d2nr05522h

rsc.li/nanoscale

Mucus-inspired organogel as an efficient absorbent and retention agent for volatile organic compounds†

Jihoon Han, ‡[a] Jemin Lee,‡[b] Seonghyeon Kim,[b] Anna Lee, [b] Hyung Gyu Park*[b] and Youn Soo Kim *[a]

Nasal mucus plays a key role in the sense of smell by absorbing and transporting chemicals to olfactory receptors. Inspired by the physical properties of mucus that enable it to transport molecules despite its high viscosity, we developed a polymeric organogel with similar viscosity and analyzed its general performance. Through qualitative and quantitative analysis, we confirmed that the matrix viscosity mainly affects the absorption and retention of volatile organic compounds (VOCs) and not their diffusion inside the matrix. Additionally, the vapor pressure of VOCs influences the absorption and retention efficiencies of the matrix. Finally, a detailed understanding of the properties of mucus along with the use of sol–gel transition enabled us to create an efficient VOC absorbent and retention agent.

[a]*Department of Materials Science and Engineering, Pohang University of Science and Technology (POSTECH), 77 Cheongam-Ro, Nam-Gu, Pohang, Gyeongbuk, 37673, Republic of Korea. E-mail: ysookim@postech.ac.kr*
[b]*Department of Mechanical Engineering, Pohang University of Science and Technology (POSTECH), 77 Cheongam-Ro, Nam-Gu, Pohang, Gyeongbuk, 37673, Republic of Korea. E-mail: parkhg@postech.ac.kr*

† Electronic supplementary information (ESI) available. See DOI: https://doi.org/10.1039/d2nr05522h

‡ These authors contributed equally to this work.

Youn Soo Kim

Youn Soo Kim has been an Assistant Professor in the Department of Materials Science and Engineering at POSTECH since 2017. She received her B.S. (2009) and M.S. (2011) degrees in chemistry and nanoscience from Ewha Womans University in Korea. She received her Ph.D. degree in chemistry and biotechnology from the University of Tokyo in 2015 and worked as a Postdoctoral Researcher at the University of Tokyo from 2015 to 2017. Her current research interests include the self-assembly of block copolymers and the synthesis of functional hydrogels to develop biomimetic soft materials, bioelectronics, and bioadhesives.

1 Introduction

Mucus is mainly composed of water and charged, high-molecular-weight glycosylated proteins known as mucins.[1,2] The mucins are covalently crosslinked *via* reversible interactions, such as hydrophobic and electrostatic interactions, to alter the viscosity and facilitate gelation.[1,2] They enable the dissolution of lipophilic odorants, such as volatile organic compounds (VOCs), in mucus that otherwise exhibits poor solubility in water.[3,4] Mucus absorbs and retains odorants that enter the nasal cavity and transports them to the olfactory receptor. Further, mucus contains antigenic substances that contribute to the protection of the human body.[5,6] As the sense of smell deteriorates as mucus dries, mucus needs to coat the nasal cavity with a viscosity optimal for balancing its drainage and secretion.[7,8] In general, mucus exhibits a viscosity in the range of 10^{-2}–10^{3} Pa s under rheometric conditions of 10^{2}–10^{-4} Hz.[9,10] Although viscosity increases hydrodynamic interaction and frictional resistance, absorbed odorants can effectively diffuse through the viscous nasal mucus to the olfactory receptors. To understand this physical property of mucus, we established a method for fabricating an organic gel matric that mimics mucus by synthesizing a block copolymer capable of forming a cross-linked network. As VOCs are soluble in dimethyl sulfoxide (DMSO) and it is less volatile than water, it was selected as the solvent to enhance the absorption and retention of VOCs. We characterized the amount of odorant absorbed into and desorbed from the matrix of the synthesized mucus with respect to viscosity and determined the diffusion coefficient of VOCs in the matrix. The results showed that with increasing matrix viscosity, VOC absorption decreased while retention increased (Fig. 1a(i)). Particularly,

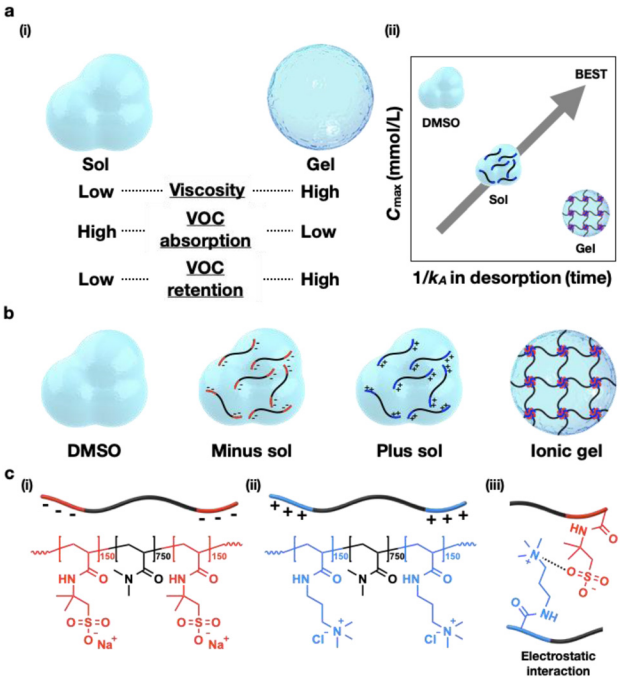

Fig. 1 (a) Schematic showing the (i) physical properties of sol and gel and (ii) maximum absorption capacity (C_{max}) according to the reciprocal of the Avrami rate constant ($1/k_A$) for VOCs desorption of samples with differing viscosity. (b) Schematic of a pure solvent (DMSO), anionic (minus sol) and cationic (plus sol) block polyelectrolyte dissolved solutions, and gel formed by mixing minus sol and plus sol (ionic gel). (c) Chemical structures of the triblock polyelectrolytes and their electrostatic interaction; poly(APTC), poly(AMPS), and poly(DMA) were used as the cationic (blue), anionic (red), and neutral (black) blocks, respectively. The triblock polyelectrolytes consist of terminal ionic blocks separated by neutral blocks.

higher matrix viscosities corresponded to lower values of the maximum absorbed VOC concentration (C_{max}) and VOC desorption rate (Fig. 1a(ii)). Finally, the C_{max} of the matrix was maximized and the desorption rate was minimized by absorbing VOCs from the sol and immediately gelating using a sol–gel transition, resulting in an efficient absorbent and retention agent.

2 Results and discussion

Among the several bonds that can create reversible cross-linking points through physical interactions that mimic mucus, electrostatic interactions of ionic polymers were effective for gelation in DMSO. Therefore, we designed an ionic ABA triblock polyelectrolyte to mimic mucus that gels through the electrostatic interaction of mucins.[1,2] ABA triblock polyelectrolytes were synthesized *via* a one-pot aqueous reversible addition fragmentation chain transfer (RAFT) polymerization (Fig. 1b and c) (details of the synthesis procedure are provided in the ESI†).[11,12] We characterized the polymerization degrees and molecular weights of the as-synthesized polymers using nuclear magnetic resonance (NMR) and gel permeation chromatography (GPC) (Fig. S1, S2 and Tables S1–S3†). To generate a sol and gel within the range of mucus viscosity,[9,10] we used a DMSO solution containing 5 wt% of a cationic or anionic block polyelectrolyte (sol). Furthermore, an ionic gel was prepared by mixing both 5 wt% cationic (plus sol) and anionic (minus sol) block polyelectrolyte solutions.

Although there is no notable difference in viscosity between the DMSO (1.2 mPa s) and sols (15.7 mPa s for the minus sol and 15.1 mPa s for the plus sol), the gel (110.1 mPa s) exhibits an evident increase in viscosity (Fig. 2a). This can be explained using the Mark–Houwink equation ($\eta = KM^{\alpha}$): polymer viscosity is proportional to the hydrodynamic coil expansion factor (α), which represents the affinity between the polymer and the solvent as well as the molecular weight (M) of the polymer.[13] In particular, even at the same polymer concentrations, the gel viscosity can be much higher than that of the sol because the three-dimensional network can restrict the polymer from stretching or aligning with the flow. Additionally, owing to the strong interaction between the polymer and the solvent, the freezable solvent molecules do not freeze.[14] To verify the

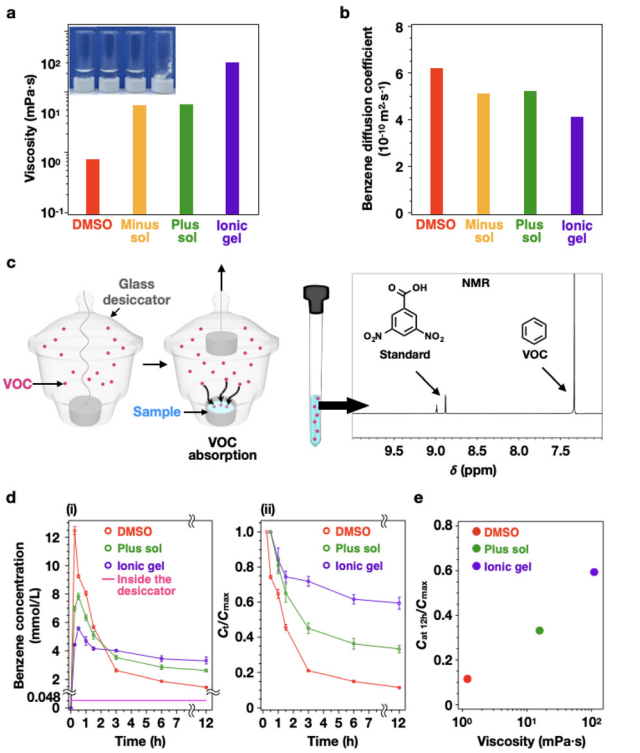

Fig. 2 (a) Viscosity of the DMSO, sols, and gel measured by a rheometer. Inset shows the photographs of inverted vials to compare the viscosity of the samples. (b) Diffusion coefficient of benzene in the matrix measured by a 2D DOSY experiment. (c) Schematic of the experimental conditions of the VOC absorption in the matrix (left) and the quantitative and qualitative analyses of VOCs present in the matrix confirmed by NMR spectroscopy (right). (d) (i) Benzene concentration and (ii) the normalized concentration (C_t/C_{max}) as a function of time. Benzene concentration in the desiccator was 0.048 mmol L^{-1}. (e) Benzene retention efficiency as a function of viscosity over the experimental time range.

solvent affinity of the polymer, we employed a differential scanning calorimeter (DSC) to measure the ratio of freezing solvent molecules to non-freezing solvent molecules (Fig. S3a†). All the matrices exhibited similar values for the proportion of non-freezing solvent, indicating that the solvent molecules are bound to the polymers (Fig. S3b†).

Next, we obtained the diffusion coefficients of VOCs in the matrices using two-dimensional (2D) diffusion-ordered spectroscopy (DOSY) (Fig. S5†). We selected the probe VOC species to avoid the overlap of its peaks in the ^{1}H NMR spectrum with those of the NMR reference and polymer (Fig. S4†). We performed the experiment using benzene, a basic aromatic VOC that satisfies the aforementioned condition. The diffusion coefficient of benzene in DMSO was confirmed by the Stokes–Einstein Gierer–Wirtz estimation (SEGWE) (details of the equation are provided in the ESI†).[15] The diffusion coefficients in various matrices are 6.17×10^{-10} m^2 s^{-1} for DMSO, 5.12×10^{-10} m^2 s^{-1} for minus sol, 5.22×10^{-10} m^2 s^{-1} for plus sol, and 4.10×10^{-10} m^2 s^{-1} for ionic gel (Fig. 2b). Although the viscosity values of the matrices increase 10-fold in the order of DMSO, sol, and gel, the diffusion coefficients of benzene in the same matrices exhibit relatively small variations within the same order of magnitude (10^{-10} m^2 s^{-1}). In general, the decrease in the diffusion coefficient in the matrix can be attributed to the obstruction effect, in which the diffusion path length of the solute increases due to impenetrable obstacles, such as polymer networks.[16] However, the obstruction effect can be negligible when the probe molecules are much smaller than the correlation length (ξ) (or mesh size) of the polymer network.[17–19] For the obstruction effect to occur, the correlation length of the polymer network must be smaller than or equal to the probe molecule sizes. As mentioned previously, our gel matrix contains a core formed by electrostatic interactions between the terminal ionic blocks of triblock polyelectrolytes, which are connected by neutral blocks (Fig. 1b and c). As the bridge is a linear polymer with 750 linked DMA units (Fig. 1c((i) and (ii)) and Tables S1–S3†), the correlation length of the gel matrix is much larger than that of the benzene molecule. Particularly, the obstruction effect in the gel matrix is negligible, and the diffusion coefficient does not differ considerably from that of the DMSO.

After that, the following experiments were prepared to confirm the absorption and retention of benzene according to the type of matrix. First, we placed a lid-covered glass dish containing 0.6 mL of DMSO, sol, and gel in a glass desiccator (Fig. 2c) as glass does not have a strong affinity for VOCs. Next, we loaded 1121 μmol of benzene in the desiccator for spontaneous vaporization. All experiments were performed in a sealed desiccator, which is a leak-free closed system. Our computational fluid dynamics (CFD) simulation indicated that the spontaneous vaporization of 1121 μmol of benzene can produce an equilibrium concentration of 1070 ppm (0.048 mmol L^{-1}) in a glass desiccator after 2 h (Fig. S6†), which agrees with the results of the direct measurement of benzene concentration using a commercial VOC sensor. Upon reaching the equilibrium benzene concentration, the lid of the glass dish containing the matrix sample was removed to initiate benzene absorption by the matrix. The amount of benzene present in each matrix was quantitatively and qualitatively characterized using an internal standard (3,5-dinitrobenzoic acid), which was added to each matrix in advance, and ^{1}H NMR spectroscopy. Through these methods, the concentration of benzene absorbed in each matrix was monitored over time (Fig. 2d(i) and Fig. S7a–c†). As the peaks of the polymer and benzene overlap in the ^{1}H NMR spectrum, the experiment was not conducted with the anionic sol matrix (Fig. S8†).

For DMSO, the maximum concentration of absorbed benzene (C_{max}, 12.5 mmol L^{-1}) appears at 15 min and then decreases rapidly, reaching 1.4 mmol L^{-1} after 12 h. In contrast, the plus sol and ionic gel exhibit a lower maximum absorption concentration (7.8 mmol L^{-1} for plus sol and 6.0 mmol L^{-1} for ionic gel) after 30 min. However, the decrease in the benzene concentration occurs smaller for both matrices than for DMSO. The concentrations of benzene in the plus sol and ionic gel are 2.8 and 3.4 mmol L^{-1} after 6 h and 2.6 and 3.3 mmol L^{-1} after 12 h, respectively, with an equilibration time of 6 h. As shown in Fig. 2d(ii), all three matrices display a two-step decreasing pattern for the time-dependent change in the benzene concentration at a specific time (C_t) for C_{max}. That is, the C_t/C_{max} value decreases rapidly initially and then gradually decreases. The C_t/C_{max} value of benzene in DMSO decreases sharply to 21% after 3 h then gradually decreases until only 12% of the C_{max} value remains after 12 h. In the plus sol, the C_t/C_{max} value decreases by 45% over 3 h then gradually decreases until only 33% of the C_{max} value remains after 12 h. In the ionic gel, the C_t/C_{max} value of benzene decreases by only 74% over 2 h. After 12 h, 59% of the C_{max} value remained in the gel, with the largest residual amount of the three matrices.

DMSO absorbs a large amount of benzene in a short time but simultaneously releases a large amount, poorly retaining the absorbed benzene. In contrast, from the plus sol to the ionic gel, the initial absorption amount of benzene decreases but is not easily released; thus, the ability to retain benzene over a long period is improved. Moreover, the retention efficiency ($C_{at\ 12\ h}/C_{max}$) of absorbed benzene is significantly different depending on the viscosity of the matrix (Fig. 2e). The matrices with the lowest viscosities (DMSO) exhibited the lowest retention efficiencies. Comparatively, with an increase in the viscosity of plus sol and ionic gel, the retention efficiency increases proportionally with the viscosity.

To confirm the absorption effect of benzene based on the type of polymer constituting the matrix, a neutral polymer solution (14.8 mPa s) and neutral gel (99.1 mPa s) with similar viscosities as those of plus sol and ionic gel were prepared (Fig. S9a–c†). Similarly, the diffusion coefficient of benzene in the matrix and the amount of absorption of vaporized benzene with time were measured. The diffusion coefficient was 5.19×10^{-10} m^2 s^{-1} for the neutral sol and 4.06×10^{-10} m^2 s^{-1} for the neutral gel, which agreed with the result of the plus sol and ionic gel, respectively (Fig. S9d†). The C_{max} values of benzene were 8.0 mmol L^{-1} for the neutral sol and 5.5 mmol L^{-1} for

the neutral gel, reached after 30 min (Fig. S9e(i), S7d, and S7e†). Additionally, the concentrations of benzene in the neutral sol and neutral gel were 2.5 and 3.0 mmol L^{-1} after 6 h and 2.1 and 2.9 mmol L^{-1} after 12 h, respectively, similar to the results of the plus sol and ionic gel. The retention efficiency ($C_{at\ 12\ h}/C_{max}$) of absorbed benzene was 27% for the neutral sol and 51% for the neutral gel (Fig. S9e(ii) and S9f†). Therefore, the diffusion coefficient, absorption amount, and retention efficiency of benzene in the matrix are the same if they exhibit the same viscosity, regardless of the matrix type. All the sol and gel matrices were composed of greater than 90% DMSO and no specific interactions, such as electrostatic attraction, cation–pi bonding, or hydrogen bonding, occurred between the trace amounts of polymer and benzene molecules. Therefore, only the solubility of benzene in DMSO and diffusion due to the difference in the concentration of benzene between the matrix and air are considered to cause benzene absorption into the matrix.

In addition, the effects of an increase in viscosity with an increase in polymer concentration on benzene absorption and retention efficiency were investigated. We prepared 5, 10, and 15 wt% ionic gels and measured the mechanical properties of the ionic gels using a rheometer (Fig. S10†). As the polymer concentration of the ionic gel increased, its mechanical strength improved. In particular, the storage moduli (G') of the 5 wt% ionic gel were higher than the loss moduli (G'') in all frequency and temperature ranges although it possessed a flowing property. Next, the benzene absorption experiment was performed with the ionic gel having a high polymer concentration. For 10 wt% (890.5 mPa s) and 15 wt% (2820.2 mPa s) ionic gels, the maximum concentration of absorbed benzene (C_{max}, 1.14 mmol L^{-1} for 10 wt% and 0.99 mmol L^{-1} for 15 wt%) appears at 60 min (Fig. S11 and S12a(i)†). The concentrations of benzene in the 10 and 15 wt% ionic gels were, respectively, 0.81 and 0.80 mmol L^{-1} after 6 h and 0.75 and 0.79 mmol L^{-1} after 12 h. The retention efficiency ($C_{at\ 12\ h}/C_{max}$) of absorbed benzene was 66% for the 10 wt% ionic gel and 80% for the 15 wt% ionic gel (Fig. S12a(ii) and S12b†). Therefore, with an increase in the ionic gel viscosity, the amount of absorption decreases but the retention efficiency increases.

An increased matrix viscosity hinders the absorption of benzene but favors its retention. This is attributed to the creation of a polymer layer with reduced porosity at the interface between the viscous matrix and air, which functions as a sieving interface. It has been reported that the surface structure of the gel at the interface between the gel and the liquid exhibits significantly lower porosity than the internal structure of the bulk gel.[20] Previous studies have shown that polystyrene microspheres with radii of 14 nm that can diffuse in the bulk gel could not penetrate the interface between the gel and the solution.[21] Additionally, the interfacial layer present on the gel surface reduces the diffusion coefficient of nanometer solutes for steric reasons and acts as a sieve to prevent penetration from the solution to the gel.

Different structures between the interface and bulk of our gel were identified by scanning electron microscopy (SEM). The ion gel was formed into a sphere and lyophilized, and then a portion was taken from the upper right part and analyzed by SEM (Fig. 3a and b(i)). From the SEM image, the surface of the gel at the interface between the gel and air exhibits a significantly reduced porosity compared with that of the inside of the gel (Fig. 3b(ii and iii)). In addition, the SEM measurements indicate the further decreased porosity of the interface sieving layer as the viscosity of the ionic gel increased (Fig. S13†).

When a three-dimensional network structure surrounds the entire matrix, a dense layer containing entangled polymer chains covers the surface of the gel at the interface between the gel and air. This is attributed to an increase in the cohesive force between the polymers that maintains the interface between different phases, such as air and gel. In addition, the evaporation of DMSO constituting the gel may enable an increase in the concentration of the polymer to occur on the surface of the gel. As a result, the polymer may become more densely entangled at the gel and air interface. Consequently, owing to the sieving interphase present on the gel surface, the diffusion properties of the gel at the interface differ from those of the gel in the bulk phase, which can significantly affect the maximum absorption and retention efficiency of VOCs (Fig. 3c(i and ii)). In the case of DMSO, benzene is rapidly absorbed from the air into DMSO because diffusion occurs due to the concentration gradient ($C_{at\ 0\ min}$ in DMSO is zero and $C_{at\ 0\ min}$ in the air is 0.048 mmol L^{-1}) in the initial stage of absorption. However, as the direction of this concentration gradient is quickly reversed ($C_{at\ 15\ min}$ in DMSO is 12.5 mmol L^{-1} and $C_{at\ 15\ min}$ in the air is 0.048 mmol L^{-1}), the concentration of benzene in DMSO rapidly decreases over time (Fig. 2d). In the case of the gel, the initial absorption C_{max}

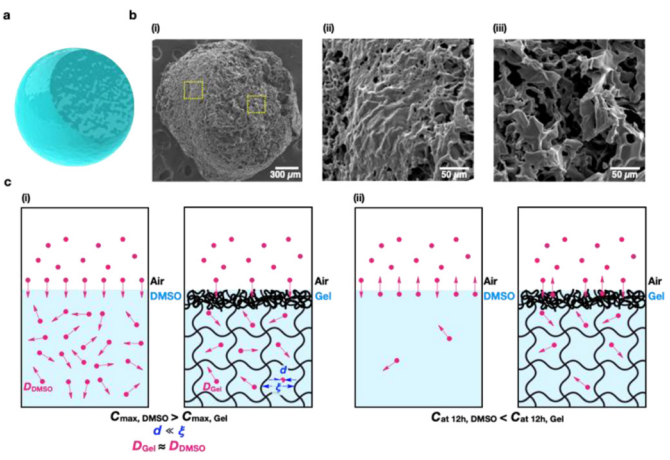

Fig. 3 (a) Schematic of a spherical ionic gel particle with the upper right portion removed for SEM measurements. (b) SEM images of the (i) entire structure of the ionic gel with a concentration of 5 wt%, (ii) reduced pore size at the interface, and (iii) increased internal pore size. The yellow dotted box indicates the magnified portion. (c) Schematic of the differences in the gas absorptions and retention mechanisms of DMSO and the gel (i) during the initial absorption and (ii) after 12 h. (*d*: diameter of molecules, ξ: correlation length, *D*: diffusion coefficient).

value is lower than that of DMSO because the sieving interphase hinders the absorption of benzene into the gel. In contrast, despite the inverse concentration gradient, the concentration of benzene in the gel is well maintained owing to the sieving interphase. In the case of the polymer sol, the sieving effect decreased owing to insufficient viscosity and the absence of a network structure to encompass the matrix.

Based on the aforementioned results, the pathway of odorants in viscous mucus in the olfactory system can be interpreted as follows. Odorants penetrate through the sieving interphase present at the mucus/air interface and diffuse through the mucus. As the diffusion coefficient of the odorants is not affected by the surrounding viscosity (Fig. 2b), the diffusion of odorants is facile. Particularly, even if the number of permeating odorants is small because of the sieving interphase of the mucus, as long as they penetrate the mucus, they can easily reach the nasal receptors.

To confirm these effects of the sieving interphase and diffusivity of the absorbents, we characterized the time evolution of VOCs (alcohol) transfer through DMSO and ionic gel. As illustrated in Fig. 4a, a nylon membrane filter coated with matrices (Fig. S14†), *e.g.*, DMSO or ionic gel (5 wt%), connects the VOCs flow line with a commercial alcohol sensor. The data acquisition begins with the first voltage response while the alcohol vapor stream flows continuously. As the noise of the output voltage fluctuated within 10 mV, a valid response of alcohol vapor appears over 30 mV, in accordance with the criteria of a signal-to-noise ratio (SNR) of 3 (Fig. 4b). For both DMSO and ionic gel, it takes 45 s for alcohol molecules to reach the sensor upon passing through the matrix-laden nylon membrane. This lag-free arrival indicates that, as mentioned previously, the diffusion coefficients inside the matrices are similar regardless of the disparity in viscosity. Contrastingly, the number of alcohol molecules, *i.e.*, relative voltage response, in DMSO tends to be higher than that in ionic gel, which can be ascribed to the sieving interphase effect. Consequently, the amount of the absorbed VOC molecules at the interface mainly depends on the sieving interphase. Once VOC molecules pass the sieving interphase, they diffuse at a similar rate regardless of the surrounding viscosity.

DMSO has a large maximum absorption of VOCs, whereas the ionic gel has a large VOC retention efficiency. However, each advantage could be obtained independently. A sensor with high sensitivity, such as the nasal receptor, can detect minimal amounts of VOCs. Nevertheless, to detect VOCs using a wide range of artificial sensors, the selected matrix must have a high VOC absorption and retention. Therefore, to develop a matrix that is both an efficient absorbent and retention agent, we focused on combining the large absorption capacity of DMSO and the high retention efficiency of the gel by utilizing the sol–gel transition. As shown in Fig. 5a, after the absorption of VOCs in DMSO reaches the maximum absorption amount, the plus and minus sols are added immediately for gelation. To maximize the sieving interphase of the ionic gel, the polymer concentration was increased to 15% and the experiments were performed in an open system. The desorption of VOCs was predominant, with the concentration gradient maximized to accurately determine the retention efficiency of VOCs in the ionic gel and DMSO. In addition, the same experiment was performed using toluene and *o*-, *m*-, and *p*-xylene, which are aromatic VOCs similar to benzene, to characterize the absorption and retention efficiency with respect to VOC vapor pressure. The vapor pressures of the VOCs are related as follows: benzene (12.7 kPa) > toluene (3.8 kPa) > xylene (0.9–1.2 kPa).[22] The VOCs were initially absorbed in DMSO in a closed system for 15 min, which is the required time to reach the maximum absorption for all the VOCs (Fig. S7a and S15†). Subsequently, the matrix sample was transferred to an open system and the VOC concentration in the matrix over time was measured (Fig. S16–S20†). In Fig. 6a–e, the VOC concentration change curve of the ionic gel remains higher than that of DMSO regardless of VOC type. This indicates that the desorption of VOCs is suppressed in the ionic gel in an open system. In addition, the lower the vapor pressure of VOCs, the lower the C_{max} in DMSO (12.5 mmol L^{-1} for benzene, 3.7 mmol L^{-1} for toluene, 2.7 mmol L^{-1} for *o*-xylene, 2.6 mmol L^{-1} for *m*-xylene, and 2.8 mmol L^{-1} for *p*-xylene). Furthermore, the difference in the number of retained VOCs between the DMSO and ionic gel decreased.

Desorption plays a key role in the decrease in the VOC concentration over time. We analyzed the desorption kinetics of the VOCs using the Avrami fractional-order kinetic model under the assumption of homogeneous desorption (for detailed information on the formula, see the ESI†). The Avrami kinetic constant (k_A) shows the rate of the desorption of VOCs

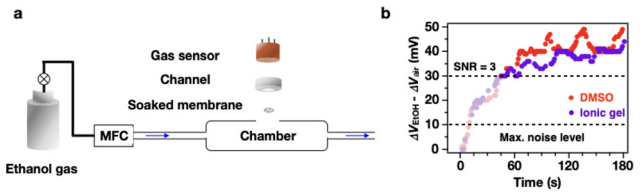

Fig. 4 (a) Schematic of the experimental conditions for real-time VOC detection. (b) Relative voltage response of the alcohol sensor with the time of ethanol vapor injection. Data of the signal-to-noise ratios (SNR) of 3 or higher are considered as valid signals; invalid data for SNR < 3 are plotted in lighter shades of the colors.

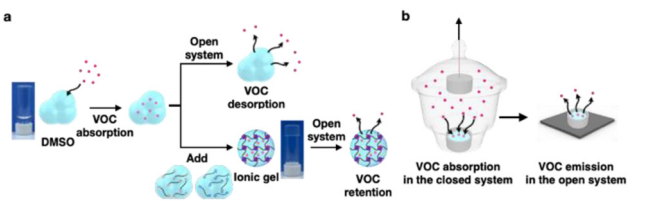

Fig. 5 (a) Mechanism of the absorption and desorption of VOCs from the DMSO and mechanism of the retention of the VOCs through forming an ionic gel. (b) Schematic of experimental conditions in the open system.

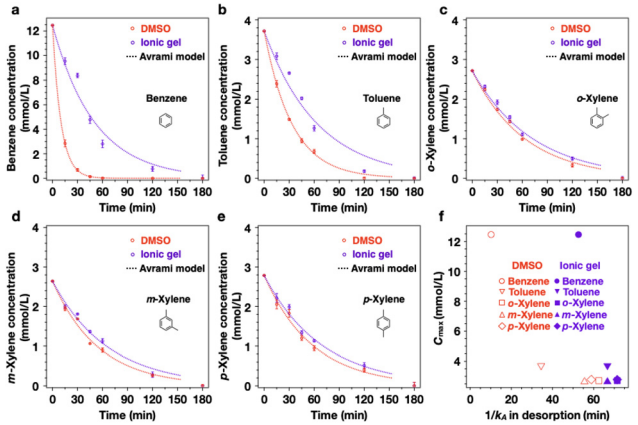

Fig. 6 (a) Benzene, (b) toluene, (c) *o*-xylene, (d) *m*-xylene, and (e) *p*-xylene concentrations in the matrices with respect to time in an open system. (f) Maximum absorption concentration (C_{max}) with respect to the reciprocal of the Avrami constant ($1/k_A$).

from the matrix. As shown in Table 1, the highly volatile VOC benzene exhibits a higher k_A in DMSO than in the ionic gel by a factor of 5. In contrast, the VOCs with low vapor pressures, such as xylene, exhibit insignificant differences in the k_A values between the two absorbents. The vapor pressure is an indication of an evaporation rate; molecules with low vapor pressure have strong intermolecular interactions with each other.[23] Therefore, VOCs with low vapor pressure will have a low evaporation rate owing to strong intermolecular interactions, regardless of the viscosity of the matrix. Eventually, the difference in VOC retention between DMSO and the ionic gel will be reduced. The relationship between $1/k_A$ and C_{max} describes the outcomes of VOCs with different volatilities according to the matrix viscosity (Fig. 6f). In addition, to facilitate a comparison with sol (absorption)–sol (retention) and sol (absorption)–gel (retention) explained above, gel (absorption)–gel (retention) was also analyzed. The VOCs were initially absorbed in 15 wt% ionic gel in the closed system for 60 min; we investigated the change in VOC concentration in the open system (Fig. S21 and S22†). As expected, owing to the high viscosity of the 15 wt% ionic gel, the amount of absorption was decreased when compared with DMSO. The values of C_{max} in the 15 wt% ionic gel were 0.99, 0.54, 0.50, 0.51, 0.49 mmol L^{-1} for benzene, toluene, *o*-xylene, *m*-xylene, and *p*-xylene, respectively. Even though the initial gel state absorbed a smaller amount of VOCs, if the viscosity of the matrix was similar, the Avrami kinetic constant (k_A) of the desorption of VOCs indicated similar values, as presented in Table S4.†

Notably, the VOC vapor pressure influences the initial absorption cavity of the matrix, whereas the viscosity of the matrix determines the VOC retention efficiency. These results demonstrate that the sol–gel transition leverages the characteristics of the absorbents to maximize the absorption and retention of the volatile VOCs.

Table 1 Avrami kinetic model parameters in the open system

	k_A (min^{-1})		R^2		$1/k_A$ (min)	
VOC	DMSO	Ionic gel	DMSO	Ionic gel	DMSO	Ionic gel
Benzene	0.098	0.019	0.999	0.999	10.204	52.631
Toluene	0.029	0.015	0.999	0.999	34.483	66.667
o-Xylene	0.016	0.014	0.990	0.983	62.500	71.429
m-Xylene	0.018	0.015	0.988	0.988	55.556	66.667
p-Xylene	0.017	0.014	0.986	0.986	58.824	71.429

3 Conclusions

In conclusion, inspired by the properties of nasal mucus, we designed polymer sol and gel and created a matrix that efficiently absorbed VOCs with high retention. At high matrix viscosities, the maximum absorption amount is low but the retention efficiency is high. Additionally, by measuring the time taken by the VOCs that permeated the matrix to reach the sensor, we showed that penetrating VOCs could diffuse into the sensor at the same rate, regardless of the matrix viscosity, as they exhibited similar diffusion coefficients. Therefore, we confirmed that the viscosity of the matrix related to the sieving interphase is critical for determining the absorption and retention efficiency. Furthermore, the higher the vapor pressure of VOCs, the higher the desorption rates and the more significant the difference in retention efficiency, which was attributed to a greater influence of the sieving interphase due to increasing the matrix viscosity. Furthermore, we generated maximum VOC absorption and retention efficiency simultaneously by introducing the sol–gel transition. This understanding of mucus would aid in the development of matrices for applications in gas absorption, storage, and real-time concentration verification. Moreover, these mucus-inspired gels that act as efficient absorbents and retention agents can expand the types of sensors that can detect volatile VOCs and broaden the detection conditions.

4 Experimental section

4.1 NMR spectroscopy

^{1}H NMR spectra were recorded on a Bruker Avance III 500 spectrometer at 25 °C and a frequency of 500 MHz. The delay time was set to 2.5 s. All the polymer and gel samples were prepared in deuterated DMSO and D_2O. Chemical shift values (δ) were reported in ppm.

4.2 2D DOSY experiment

The 2D DOSY experiment was performed at 298 K on a Bruker Avance III 600 spectrometer and the data were processed using TOPSPIN 3.1 (Bruker). The total gradient duration was 2 ms and the diffusion delay was 100 ms. Gradient intensities varied geometrically from 1 to 5.35 G mm^{-1}. We acquired 16 1D spectra, with 16 scans/experiment.

4.3 VOC concentration determination

For determining the VOC concentration, 3,5-dinitrobenzoic acid was used as an internal standard. For measurement accuracy, the standard was dissolved in deuterated DMSO at a concentration of 0.1 g mL^{-1} and 10 μL was added to the sample. The volume of the sample was fixed at 0.6 mL, and the volume of the desiccator was 23.5 L. As the exact concentration of the standard was known, the VOC concentration was quantified by comparing the integrated intensity of the standard protons (δ = 9.1–8.8 ppm, 3 H) with those of the VOC protons of benzene (δ = 7.37–7.34 ppm, 6 H), toluene without methyl protons (δ = 7.30–7.10 ppm, 5 H), *o*-xylene without methyl protons (δ = 7.15–7.00 ppm, 4 H), *m*-xylene without methyl protons (δ = 7.20–6.90 ppm, 4 H), and *p*-xylene without methyl protons (δ = 7.06–7.03 ppm, 4 H). All the VOCs were vaporized in the desiccator by 1121 μmol. The added amounts of neat VOC solvent are as follows: benzene (99.9 μL), toluene (119.1 μL), *o*-xylene (135.4 μL), *m*-xylene (138.4 μL), and *p*-xylene (138.2 μL).

4.4 Rheological measurements

Rheological experiments were performed on a DHR-2 rheometer (TA Instruments) using a 4° cone plate with a diameter of 20 mm. The rheometer was equipped with a Peltier heating system containing an environmental enclosure for temperature control. Viscosity measurements were performed at a constant shear rate of 100 s^{-1} and temperature of 25 °C, with a measuring time of 5 s per point. A frequency sweep was conducted at frequencies ranging from 0.1 to 40 rad s^{-1} and temperatures ranging from 10 to 60 °C at a strain of 1%.

4.5 SEM observations

To prepare samples for SEM analysis, the ionic gel was rapidly frozen in liquid nitrogen and freeze-dried at a temperature of −50 °C and pressure of 0.1 Pa for 3 days using a freeze dryer (HyperCOOL HC3055, GYROZEN). Before SEM observations, the surfaces of the freeze-dried PEC hydrogels were coated by platinum (PT) sputtering. The internal and interface structures of the freeze-dried ionic gel were observed using SEM (JSM-7800F Prime, JEOL Ltd) at an accelerating voltage of 15 kV.

4.6 Real-time VOC detection

For real-time VOC detection, we used a custom-made gas-sensing system consisting of a vapor generator, mass flow controller (MFC), and sensing chamber. The vapor generator was a stainless-steel cylinder with an internal volume of 20 L. Initially, the cylinder was filled with a small amount, for example, 50–100 μL, of VOC solvent and air up to 1 bar of total cylinder pressure; the amount of the VOC solvent determined the partial pressure of the input vapor. The MFC (MF-200C, MFC FLOW) provides a VOC-laden air flow to the sensing chamber at 100 sccm. We designed and 3D-printed the sensing chamber with an internal volume of approximately 11 000 cm^3. At the top of the chamber, a circular nylon membrane filter (7402-004, Whatman, Schleicher & Schuell) with a diameter of 9 mm and pore widths of 200 nm delivered the VOC molecules to the sensor. A commercial alcohol sensor (MQ-3, Hanwei Electronics) measured the concentration of the VOC based on the change in the output voltage. At the high temperature generated by the internal heating coil, oxygen was adsorbed on the SnO_2 surface of the alcohol sensor. This adsorption creates an electron depletion layer on the SnO_2 surface so that the output voltage drops. As soon as the alcohol molecules come in, they react the oxygen away and lower the potential barrier. Therefore, the output voltage increases. Thus, ΔV indicates the difference between voltage output with and without the blowing gas. We added 10 μL of DMSO or ionic gel to the membrane filter to enable the VOC molecules to transfer through the matrices prior to reaching the MQ-3 sensor. The voltage response of the air-only input acted as a reference value when compared with that of 1000 ppm of ethanol vapor in the same organic layer. A data acquisition system measured data every 0.5 s, and we evaluated a time-averaged response every 3 s for approximately 3 min. The noise of the voltage response data fluctuated within 10 mV. To avoid a false-positive evaluation owing to the data fluctuation, we considered relative voltage responses over 30 mV as valid data, corresponding to the signal-to-noise ratio of 3.

Author contributions

H. G. P. and Y. S. K. conceived the idea and designed the research. J. H. and J. L. performed the experiments. J. L. analyzed the data using the Avrami model. S. K. and A. L. performed the CFD simulations. All the authors contributed to the data treatment and interpretation of the results. J. H., J. L., H. G. P., and Y. S. K. wrote the manuscript. All the authors reviewed the manuscript.

Conflicts of interest

The authors have no conflicts of interest to declare.

Acknowledgements

This research was financially supported by a National Research Foundation of Korea (NRF) grant funded by the Korean Government (MSIT) (No. 2019R1C1C1002836), and by the Basic Research Program and Leader Research Program through an NRF grant funded by the MSIT (No. 2020R1A4A3079853, No. 2020R1A3B2079741). The authors would like to thank Jinwoo Lee for their assistance in using commercial alcohol sensors. We also thank Prof. Aya Mizutani Akimoto and Prof. Takamasa Sakai for the generous discussion. Prof. Hyung Gyu Park was also supported by the Institute for Basic Science (IBS-R034-D1).

References

1 B. Demouveaux, V. Gouyer, F. Gottrand, T. Narita and J. L. Desseyn, *Adv. Colloid Interface Sci.*, 2018, **252**, 69–82.
2 D. J. Thornton and J. K. Sheehan, *Proc. Am. Thorac. Soc.*, 2004, **1**, 54–61.
3 D. B. Kurtz, K. Zhao, D. E. Hornung and P. Scherer, *Chem. Senses*, 2004, **29**, 763–773.
4 P. Pelosi and S. Michele, *Crit. Rev. Biochem. Mol. Biol.*, 1994, **29**, 199–228.
5 H. Kida, Y. Fukutani, J. D. Mainland, C. A. de March, A. Vihani, Y. R. Li, Q. Chi, A. Toyama, L. Liu, M. Kameda, M. Yohda and H. Matsunami, *Nat. Commun.*, 2018, **9**, 1–10.
6 M. E. V. Johansson and G. C. Hansson, *Nat. Rev. Immunol.*, 2016, **16**, 639–649.
7 J. Gamain, T. Herr, R. Fleischmann, A. Stenner, M. Vollmer, C. Willert, B. Veit, B. Lehnert, J. U. Mueller, F. Steigerwald, F. Tost and M. Kronenbuerger, *J. Neural Transm.*, 2021, **128**, 1215–1224.
8 T. J. W. Hassell and D. Charles, *Toxins*, 2020, **12**, 269.
9 X. Wang, H. Su, W. Lv, M. Du, Y. Song and Q. Zheng, *J. Rheol.*, 2015, **59**, 51–62.
10 R. Hirose, T. Nakaya, Y. Naito, T. Daidoji, R. Bandou, K. Inoue, O. Dohi, N. Yoshida, H. Konishi and Y. Itoh, *mSphere*, 2019, **4**, e00474–e00419.
11 G. Gody, T. Maschmeyer, P. B. Zetterlund and S. Perrier, *Macromolecules*, 2014, **47**, 3451–3460.
12 G. Gody, T. Maschmeyer, P. B. Zetterlund and S. Perrier, *Nat. Commun.*, 2013, **4**, 1–9.
13 M. Rubinstein and R. H. Colby, *Polymer Physics*, Oxford University Press, 2003.
14 T. Nakaoki and H. Yamashita, *Open J. Org. Polym. Mater.*, 2016, **6**, 86–97.
15 R. Evans, G. Dal Poggetto, M. Nilsson and G. A. Morris, *Anal. Chem.*, 2018, **90**, 3987–3994.
16 A. H. Muhr and J. M. V. Blanshard, *Polymer*, 1982, **23**, 1012–1026.
17 M. A. B. H. Susan, T. Kaneko, A. Noda and M. Watanabe, *J. Am. Chem. Soc.*, 2005, **127**, 4976–4983.
18 M. Tokita, *Transport in and Through Gel*, Springer, Singapore, 2018, pp. 413–443.
19 Y. Kim, S. Joo, W. K. Kim and J. H. Jeon, *Macromolecules*, 2022, **55**, 7136–7147.
20 J. Labille, N. Fatin-Rouge and J. Buffle, *Langmuir*, 2007, **23**, 2083–2090.
21 N. Fatin-Rouge, K. Starchev and J. Buffle, *Biophys. J.*, 2004, **86**, 2710–2719.
22 S. Maken, B. R. Deshawl, Anu, K. C. Singh, S. J. Park and J. W. Park, *Phys. Chem. Liq.*, 2005, **43**, 149–156.
23 P. Atkins, J. D. Paula and J. Keeler, *Physical Chemistry*, Oxford University Press, 2018, pp. 1–940.